Photodissociation of S atom containing amino acid chromophores

Ming-Fu Lin, Yuri A. Dyakov, Yuan T. Lee,[a] S. H. Lin,[a] Alexander M. Mebel,[b] and Chi-Kung Ni[c]
Institute of Atomic and Molecular Sciences, Academia Sinica, P.O. Box 23-166, Taipei 10617, Taiwan

(Received 26 March 2007; accepted 26 June 2007; published online 13 August 2007)

Photodissociation of 3-(methylthio)propylamine and cysteamine, the chromophores of S atom containing amino acid methionine and cysteine, respectively, was studied separately in a molecular beam at 193 nm using multimass ion imaging techniques. Four dissociation channels were observed for 3-(methylthio)propylamine, including (1) $CH_3SCH_2CH_2CH_2NH_2 \rightarrow CH_3SCH_2CH_2CH_2NH + H$, (2) $CH_3SCH_2CH_2CH_2NH_2 \rightarrow CH_3 + SCH_2CH_2CH_2NH_2$, (3) $CH_3SCH_2CH_2CH_2NH_2 \rightarrow CH_3S + CH_2CH_2CH_2NH_2$, and (4) $CH_3SCH_2CH_2CH_2NH_2 \rightarrow CH_3SCH_2 + CH_2CH_2NH_2$. Two dissociation channels were observed from cysteamine, including (5) $HSCH_2CH_2NH_2 \rightarrow HS + CH_2CH_2NH_2$ and (6) $HSCH_2CH_2NH_2 \rightarrow HSCH_2 + CH_2NH_2$. The photofragment translational energy distributions suggest that reaction (1) and parts of the reactions (2), (3), and (5) occur on the repulsive excited states. However, reaction (4) and (6) occur only after the internal conversion to the electronic ground state. Since the dissociation from an excited state with a repulsive potential energy surface is very fast, it would not be quenched completely even in the condensed phase. Our results indicate that reactions following dissociation may play an important role in the UV photochemistry of S atom containing amino acid chromophores in the condensed phase. A comparison with the potential energy surface from *ab initio* calculations and branching ratios from RRKM calculations was made. © *2007 American Institute of Physics*. [DOI: 10.1063/1.2761916]

I. INTRODUCTION

The nucleic acid bases and aromatic amino acids are some of the most important biomolecules. One of the most important photophysical characteristics of these molecules is the low fluorescence quantum yield. It indicates the existence of fast nonradiative processes, which efficiently quench the fluorescence.[1–4] The nonradiative process presumably is the ultrafast internal conversion back to the electronic ground state.[2–5] As soon as the photon energy becomes vibrational energy through internal conversion, the energy is dissipated quickly to the surrounding molecules through intermolecular energy transfer before chemical reactions take place. This so-called photostability prevents the undesirable photochemical reactions of these molecules upon UV irradiation.

Phenol and indole are the chromophores of amino acids, tyrosine, and tryptophan, respectively. A recent *ab initio* calculation suggests that the low fluorescence quantum yields of these molecules could be due to the dissociative characteristic of the electronic excited state potential energy surface, instead of fast internal conversion to the electronic ground state.[6–8] The calculation shows that absorption of UV photons corresponds to the photoexcitation of phenol to the S_1 $\pi\pi^*$ excited state. The second excited state has a significant antibonding σ^* character with respect to the OH bond. The population of the bright state, S_1, can be transferred to the dark state, S_2, through a conical intersection. As a result, instead of the internal conversion to the ground electronic state, the predissociation through $\pi\pi^*$ and $\pi\sigma^*$ coupling provides the other explanation of the rapid quenching of the fluorescence. The calculation also shows that indole has the same electronic excited state properties.

Identification of these excited states and measurement of the dissociation branching ratios from these states are very important. Recent studies of photoinduced dynamics of phenol-water and phenol-ammonia clusters show that H atom transfer, instead of proton transfer is the major reaction channel. It indicates the H atom elimination from the photoexcitation of phenol.[9–18] Indeed, the H atom elimination from the repulsive electronic excited state of phenol and indole has been verified in recent molecular beam experiment.[19,20] Since the dissociation from the excited state with a repulsive potential energy surface is very fast, it would not be quenched completely even in the condensed phase. For example, the generation of phenoxy radical from the photodissociation of phenol is very efficient even in the condensed phase.[21–28] Therefore, the dissociation from the repulsive excited state and the reactions of radicals generated from dissociation in the condensed phase where most biomolecules exist naturally may play an important role in the photochemistry of phenol and indole related molecules.

In this work, we report the photodissociation of S atom containing amino acid chromophores, 3-(methylthio)propylamine and cysteamine. We demonstrate that this is the other category of amino acid chromophores where dissociation can occur directly from a repulsive potential energy surface.

[a]Also at Department of Chemistry, National Taiwan University, Taipei, Taiwan.
[b]Permanent address: Department of Chemistry and Biochemistry, Florida International University, Miami FL 33199.
[c]Author to whom correspondence should be addressed. Also at Department of Chemistry, National Tsing Hua University, Hsinchu, Taiwan. Electronic mail: ckni@po.iams.sinica.edu.tw

II. EXPERIMENT

The experimental techniques have been described in detail in our previous reports,[29–34] and only a brief account is given here. 3-(methylthio)propylamine (or cysteamine) vapor was formed by flowing ultrapure He at a pressure of 600 Torr (or 1000 Torr) through a reservoir filled with 3-(methylthio)propylamine sample at 25 °C (or 80 °C for cysteamine). The 3-(methylthio)propylamine (or cysteamine)/He mixture was then expanded through a 500 μm high temperature (110 °C) pulsed nozzle to form the molecular beam. Molecules in the molecular beam were photodissociated by UV laser pulses, and fragments were ionized by VUV laser pulses and then detected by multimass ion imaging detector.

III. COMPUTATION

In order to further investigate the dissociation mechanism of C_2H_7NS and $C_4H_{11}NS$, *ab initio* quantum chemical calculations of the ground and excited electronic state potential energy surfaces were performed. All calculations were performed employing the GAUSSIAN 03 and MOLPRO 2002 packages.

Geometry optimization for the triplet state and excited singlet state were performed using the CASSCF(11,12)/6-311+G** method. After the geometry optimization, the energies of C_2H_7NS and $C_4H_{11}NS$ were improved by the MRCI(11,12)/6-311+G** and MRCI(7,8)/6-311+G** *ab initio* calculations, respectively. In order to estimate relative errors of our MRCI calculations, more precise G3-type computational scheme,[35(a)] in particular, its G3(MP2,CC)//B3LYP modification[35(b),35(c)] was used to calculate the triplet state energies and the zero point energy (ZPE) corrections were taken into account using B3LYP/6-31G* frequencies without scaling. To avoid imaginary values of frequencies, the triplet state frequencies were used in the ground state G3 energy calculations when the ground state energies at the geometry corresponding to the optimized triplet state geometry were calculated.

In order to understand the ground state dissociation following the radiationless internal conversion, we applied *ab initio*/Rice-Ramsperger-Kassel-Marcus (RRKM) calculations. The geometries of all intermediates and transition states on the ground electronic state were fully optimized using the hybrid density functional B3LYP method[36,37] with the 6-31G* basis set.[38] Connections between transition states and corresponding local minima were confirmed by intrinsic reaction coordinate calculations. Energies of intermediates and transition states at B3LYP/6-31G* optimized geometries were calculated using the G3-type computational scheme,[35(a)] in particular, its G3(MP2,CC)//B3LYP modification.[35(b),35(c)] Zero point energy (ZPE) corrections were taken into account using B3LYP/6-31G* frequencies without scaling. G3 energies and B3LYP/6-31G* frequencies for all intermediates and transition states were used to perform the RRKM calculations. In these calculations, available internal energy was taken to be equal to the energy of a 193 nm photon absorbed by the C_2H_7NS and $C_4H_{11}NS$ molecules (148.1 kcal/mol). With all the rate constants for each transition state from RRKM calculation, we calculated product branching ratios by solving first-order kinetic equations for unimolecular reactions. Relative product yields (branching ratios) were found using the steady-state approximation, in which branching ratios can be readily found via matrix inversion after setting up the steady-state equations in matrix form. For the radical product channels, no distinct transition states exist on the PES for the last reaction step, as it is a simple bond cleavage process. In this case, we used the variational transition state theory (VTST) by considering different positions for the transition state along the reaction path, calculating rate constants corresponding to each of them and finding the minimal rate. To perform VTST calculations, the B3LYP/6-31G* energies were scaled by the ratio of energies of the products calculated at the B3LYP/6-31G* and G3 levels. Before the scaling, the basis correction term, i.e., the difference between MP2/G3MP2large and MP2/6-31G* energies, was subtracted from the G3 energies of products. These terms were calculated exactly along the dissociation channel potential energy profile and then added to the scaled B3LYP/6-31G* energies. Additional computational details of our *ab initio*/RRKM/VTST approach have been described earlier.[39]

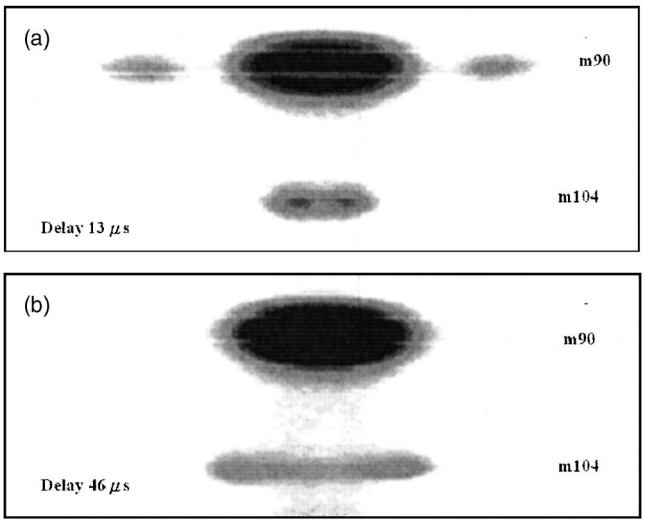

FIG. 1. Photofragment ion images from the photodissociation of 3-(methylthio)propylamine at 193 nm. The ionization wavelength is 193 nm. For the long delay time, the fast component of $m/e=90$ has flown out of the detection region.

IV. RESULTS AND DATA ANALYSIS

A. 3-(methylthio)propylamine

Fragments of $m/e=104$ and 90 were observed from the photodissociation of 3-(methylthio)propylamine at 193 nm using the 193 nm photoionization laser beam. The image of $m/e=104$ is a line shape image, as illustrated in Fig. 1. The length of the image increases rapidly with the increase of the delay time between pump and probe laser pulses. It is the product from H atom elimination with large translational energy, indicating the dissociation from a repulsive state or from a state with a large exit barrier height. Since the generation of two radicals from the ground electronic state is not expected to have a large exit barrier and the alkyl group is

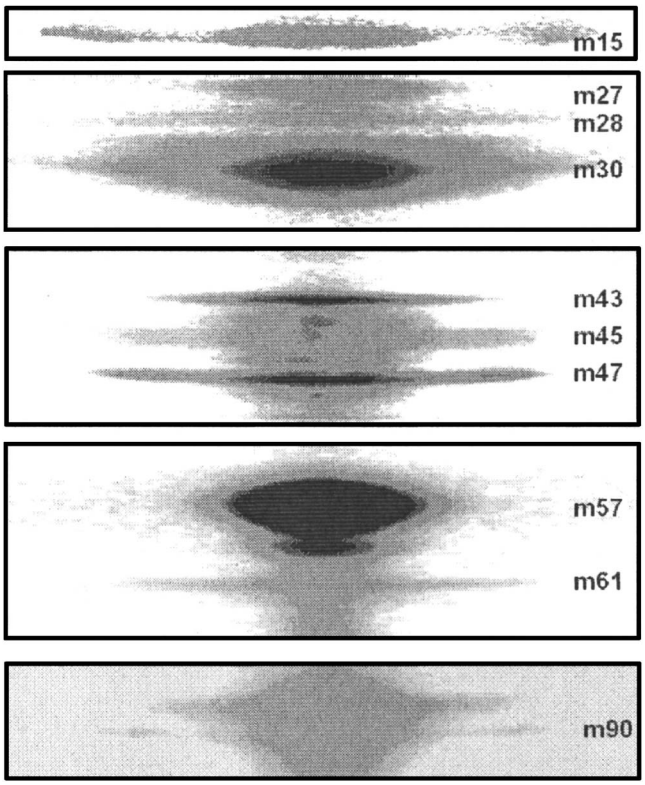

FIG. 2. Photofragment ion images from the photodissociation of 3-(methylthio)propylamine at 193 nm. The ionization wavelength is 118 nm.

not the electronic chromophore at 193 nm, H atom elimination from the alkyl group would not occur. Though both the amino group and the CH_3-S-C functionality serve as chromophores at 193 nm, the CH_3-S-C group would likely evidence S–C bond cleavage, not C–H bond cleavage, so the observed H atom elimination channel is assigned to cleavage of the N–H bond in the amino group chromophore: $CH_3SCH_2CH_2CH_2NH_2 \rightarrow CH_3SCH_2CH_2CH_2NH$ $(m=104)$ $+H$.

The image of fragment $m/e=90$ has two components. A line shape component located on both wings and a high intensity disklike component located at the center. As the delay time between the pump and the probe laser pulses increased, the component on both wings moved rapidly toward the outside. On the other hand, the size of the disklike image at the center did not change. The observed line shape component outside the disklike image must result from the fragments, $SCH_2CH_2CH_2NH_2$ $(m=90)$, corresponding to CH_3 elimination with large recoil velocity.

Fragments of $m/e=90$, 89, 61, 57, 47, 46, 45, 44, 43, 30, 29, 28, 27, and 15 were observed from the photodissociation of 3-(methylthio)propylamine at 193 nm using 118.2 nm photoionization laser beam. Fragment ion images are shown in Fig. 2. The image of fragment $m/e=90$ clearly shows three components. A line shape component located on both wings and a line shape component superimposed on a disklike component at the center. The line shape component on the wings and the line shape component at the center are the fragments that resulted from the dissociation with large recoil velocity and small recoil velocity, respectively. The disklike image was from the dissociative ionization of parent molecules by vacuum ultraviolet (VUV) photoionization due to the excess VUV photon energy. The image of $m/e=15$ shows two-line shape components. Momentum distributions of $m/e=15$ and $m/e=90$ line shape components match very well, indicating they result from the same dissociation channel, i.e., $CH_3SCH_2CH_2CH_2NH_2 \rightarrow CH_3$ $+SCH_2CH_2CH_2NH_2$.

Table I lists the dissociation barrier heights and heats of reactions of the primary and secondary dissociation channels, and various dissociative ionizations of fragments. The heavy fragment from the dissociation channel $CH_3SCH_2CH_2CH_2NH_2 \rightarrow CH_3+SCH_2CH_2CH_2NH_2$ can further dissociate into $SCH_2CH_2CH_2NH_2 \rightarrow SCH_2CH_2$ $(m=60$, ionization potential (I.P.)$=7.6$ eV$)+CH_2NH_2$ $(m=30$, I.P.$=7.0$ eV$)$ or $SCH_2CH_2CH_2NH_2 \rightarrow SCH_2CH_3$ $(m=61)+CH_2NH$ $(m=29)$, or $SCH_2CH_2CH_2NH_2 \rightarrow SCH_2$ $(m=46$, I.P.$=9.3$ eV$)+CH_2CH_2NH_2$ $(m=44)$. It can also dissociate into smaller ionic fragment after ionization $SCH_2CH_2CH_2NH_2+h\nu(118.2\ \text{nm}) \rightarrow SCH_2CH_2+CH_2NH_2^+$ $(m=30)$. However, neither fragment $m/e=60$ nor $m/e=46$ was observed. Only large intensity of $m/e=30$ and small intensity of $m/e=29$ were observed. In fact, fragments $m/e=30$ result from the other dissociation channel, as it will be discussed in the text below. The match of the momentum distributions measured for $m/e=90$ and 15 confirms that the secondary dissociation processes and dissociative ionization are negligible.

The image of fragment $m/e=61(CH_3SCH_2^+)$ has a line shape component. In addition to large intensity of $m/e=43$, we only observed a very weak intensity of the light fragment partner, $m/e=44(CH_2CH_2NH_2^+)$. However, the momentum distributions of $m/e=44$ and $m/e=43$ are the same. The small intensity of $m/e=44$ and large intensity of $m/e=43$ can be attributed to the following two reasons. First, $CH_2CH_2NH_2$ $(m=44)$ can easily decompose into smaller fragments. Our calculation shows that the heat of reaction $CH_2CH_2NH_2$ $(m=44) \rightarrow CH_2CHNH_2$ $(m=43)+H$ is 25.9 kcal/mol, and the heat of reaction $CH_2CH_2NH_2$ $(m=44) \rightarrow CH_3CHNH$ $(m=43)+H$ is 22.6 kcal/mol. In addition, the $CH_2CH_2NH_2 \rightarrow CH_2CH_2+NH_2$ reaction heat is only 15.9 kcal/mol. Second, most of the $R'-NH-R\cdot$ radicals (R, R′=H or alkyl group) have very low ionization potentials (I.P.s) and they are easily cracked into smaller ionic fragments after photoionization.[40] The heats of reactions for the dissociative ionization $CH_2CH_2NH_2 \rightarrow CH_2CHNH_2^+$ $(m/e=43)+H$ and $CH_2CH_2NH_2 \rightarrow CH_3CHNH^+$ $(m/e=43)$ $+H$ are only 9.8 and 9.5 eV, respectively. Since the 118 nm photon energy (10.5 eV) is much larger than the dissociative ionization threshold, fragments $m/e=44$ can easily crack into ionic fragment $m/e=43$ after ionization. The match of momentum distribution between $m/e=61$ and 43 indicates the $CH_3SCH_2CH_2CH_2NH_2 \rightarrow CH_3SCH_2+CH_2CH_2NH_2$ dissociation channel.

In addition to the reaction $CH_3SCH_2CH_2CH_2NH_2$ $\rightarrow CH_3SCH_2+CH_2CH_2NH_2$, fragment $m/e=61$ can be generated from the other two secondary dissociation channels. One is $CH_3SCH_2CH_2CH_2NH_2 \rightarrow CH_3+SCH_2CH_2CH_2NH_2$ $\rightarrow CH_3+SCH_2CH_3+CHNH_2$. The secondary dissociation

TABLE I. Heats of reaction and dissociation barrier heights (kcal/mol) of related reactions from *ab initio* calculations.

Reaction	ΔH	Barrier	Reaction	ΔH	Barrier
$CH_3SCH_2CH_2CH_2NH_2 \rightarrow CH_3SCH_2CH_2CH_2NH+H$	98	98	$SCH_3 \rightarrow SCH+H_2$	203	203
$CH_3SCH_2CH_2CH_2NH_2 \rightarrow CH_3SCH_2CH_2CHNH_2+H$	90	90	$SCH_2CH_2CH_2NH_2 \rightarrow SCH_2CH_2+CH_2NH_2$	26	40
$CH_3SCH_2CH_2CH_2NH_2 \rightarrow CH_3SCH_2CHCH_2NH_2+H$	96	96	$SCH_2CH_2CH_2NH_2 \rightarrow SCH_2+CH_2CH_2NH_2$	36	39
$CH_3SCH_2CH_2CH_2NH_2 \rightarrow CH_3SCHCH_2CH_2NH_2+H$	91	91	$SCH_2CH_2CH_2NH_2 \rightarrow SCH_2CH_2+CH_2NH_2^+$	171	171
$CH_3SCH_2CH_2CH_2NH_2 \rightarrow CH_2SCH_2CH_2CH_2NH_2+H$	92	92	$CH_3SCH_2CH_2CH_2 \rightarrow CH_3SCH_2+CH_2CH_2$	15.8	24
$CH_3SCH_2CH_2CH_2NH_2 \rightarrow CH_3+SCH_2CH_2CH_2NH_2$	72	72	$CH_3SCH_2CH_2CH_2 \rightarrow CH_3S+C_3H_6$	12	32
$CH_3SCH_2CH_2CH_2NH_2 \rightarrow CH_3S+CH_2CH_2CH_2NH_2$	71	71	$CH_3SCH_2CH_2CH_2 \rightarrow CH_3SCH_2^++CH_2CH_2$	175	175
$CH_3SCH_2CH_2CH_2NH_2 \rightarrow CH_3SCH_2+CH_2CH_2NH_2$	81	81	$CH_3SCH_2CH_2 \rightarrow CH_3S+CH_2CH_2$	7	9
$CH_3SCH_2CH_2CH_2NH_2 \rightarrow CH_3SCH_2CH_2+CH_2NH_2$	80	80	$CH_3SCH_2CH_2 \rightarrow CH_3+c\text{-}SCH_2CH_2$	18	18
$CH_3SCH_2CH_2CH_2NH_2 \rightarrow CH_3SCH_2CH_2CH_2+NH_2$	84	84	$HSCH_2CH_2NH_2 \rightarrow H+SCH_2CHNH_2$	86	86
$CH_2CH_2NH_2 \rightarrow CH_2CHNH_2+H$	25	25	$HSCH_2CH_2NH_2 \rightarrow HSCHCH_2+NH_3$	10	62
$CH_2CH_2NH_2 \rightarrow CH_2CH_2+NH_2$	16	16	$HSCH_2CH_2NH_2 \rightarrow HSCH_3+CHNH_2$	54	75
$CH_2CH_2NH_2 \rightarrow CH_2CHNH_2^++H$	226	256	$HSCH_2CH_2NH_2 \rightarrow HSCH_2CH_2NH+H$	99	99
$CH_2CH_2NH_2 \rightarrow CH_3CHNH^++H$	244	244	$HSCH_2CH_2NH_2 \rightarrow HS+CH_2CH_2NH_2$	73	73
$CH_2CH_2CH_2NH_2 \rightarrow C_2H_4+CH_2NH_2$	16	24	$HSCH_2CH_2NH_2 \rightarrow HSCH_2+CH_2NH_2$	76	76
$CH_2CH_2CH_2NH_2 \rightarrow C_3H_3+CH_3N\ H_2$	32	82	$HSCH_2CH_2NH_2 \rightarrow HSCH_2CH_2+NH_2$	82	82
$CH_2CH_2CH_2NH_2 \rightarrow C_2H_5+CH_3N$	51	51	$HSCH_2 \rightarrow SCH_2+H$	40	41
$CH_2CH_2CH_2NH_2 \rightarrow C_2H_4+CH_2NH_2^+$	160	160			

has barrier height of 62 kcal/mol, and the heat of reaction is 51 kcal/mol. The maximum available energy left in the primary fragment $SCH_2CH_2CH_2NH_2$ (76 kcal/mol) is very close to the barrier height of the secondary reaction. Therefore, this secondary reaction is not likely to occur. In fact, as we discussed above, the intensity of $m/e=29$ ($CHNH_2$) is weak and the contribution must be small. The other possible source of fragment $m/e=61$ is $CH_3SCH_2CH_2CH_2NH_2 \rightarrow CH_3SCH_2CH_2CH_2+NH_2 \rightarrow CH_3SCH_2+CH_2CH_2+NH_2$; however, the match of momentum distributions between $m/e=61$ and 43 suggests it is not important.

Both fragments $m/e=47$ and 45 have line shape images. They have the same image intensity profiles. Ions of $m/e=45$ must result from the dissociative ionization of $m/e=47$. Our calculation shows that the heat of reaction of dissociative ionization SCH_3 ($m=47$) $\rightarrow HCS^+$ ($m=45$) $+H_2$ is only 8.78 eV. This indicates that fragment SCH_3 can easily crack into smaller ionic fragments after ionization by 10.5 eV photon. We cannot find the corresponding heavy fragment $m/e=58$ ($CH_2CH_2CH_2NH_2$) for fragment $m=47$. However, we observed $m/e=30$, 29, 28, and 27. Since we did not find the corresponding heavy fragments for $m/e=30$, 29, 28, and 27, either, it is likely that the fragment $CH_2CH_2CH_2NH_2$ dissociates into smaller fragment due to the low dissociation threshold, or it cracks into smaller ionic fragments after ionization. Table I lists the possible dissociation channels of neutral fragment $CH_2CH_2CH_2NH_2$ as well as cation $CH_2CH_2CH_2NH_2^+$ from *ab initio* calculations. It shows that the dissociation barrier height of neutral fragment $CH_2CH_2CH_2NH_2$ ($m=58$) is as low as only 24 kcal/mol. Most of the fragments $CH_2CH_2CH_2NH_2$ can easily dissociate into smaller fragments. In addition, the ionization potential of $CH_2CH_2CH_2NH_2$ is only 8.2 eV. The cation $CH_2CH_2CH_2NH_2^+$ can easily dissociate into $C_2H_4+CH_2NH_2^+$ with the excess energy from VUV photon without barrier. This provides the explanation that fragment ions $m/e=27-30$, instead of $m/e=58$, were observed.

The other possible source of $m/e=47$ results from the secondary dissociation $CH_3SCH_2CH_2CH_2NH_2 \rightarrow CH_3SCH_2CH_2$ ($m=75$) $+CH_2NH_2 \rightarrow CH_3S$ ($m=47$) $+CH_2CH_2+CH_2NH_2$. We did not observe the fragment $m/e=75$. If it were from secondary dissociation, it has indi-

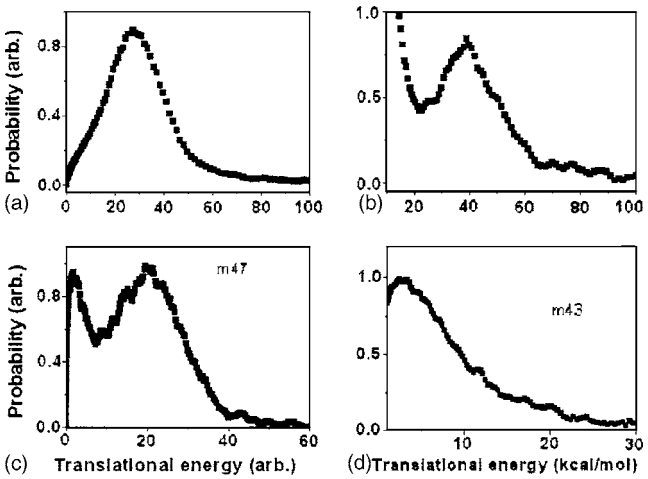

FIG. 3. Translational energy distribution of reaction (a) $CH_3SCH_2CH_2CH_2NH_2 \rightarrow CH_3SCH_2CH_2CH_2NH+H$, (b) $CH_3SCH_2CH_2CH_2NH_2 \rightarrow CH_3+SCH_2CH_2CH_2NH_2$, (c) $CH_3SCH_2CH_2CH_2NH_2 \rightarrow CH_3S+CH_2CH_2CH_2NH_2$, and (d) $CH_3SCH_2CH_2CH_2NH_2 \rightarrow CH_3SCH_2+CH_2CH_2NH_2$.

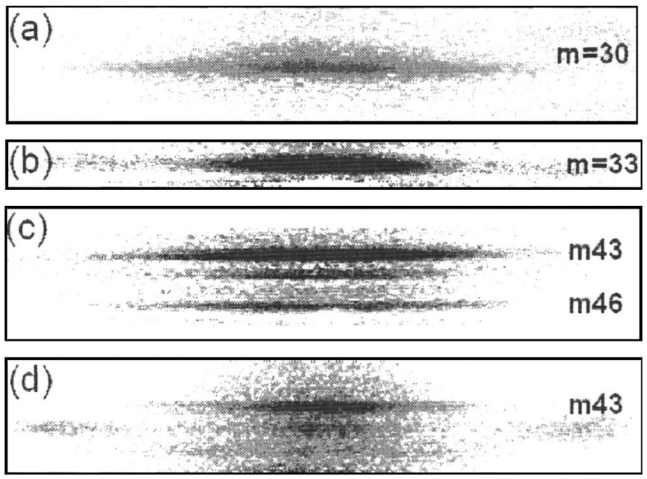

FIG. 4. Photofragment ion images from the photodissociation of cysteamine at 193 nm. The ionization wavelengths are (a) 157 nm, (b) 118 nm, (c) 118 nm, and (d) 157 nm.

cated that fragment $m/e=75$ proceeds the secondary dissociation completely. Although the final products are the same as from $CH_3SCH_2CH_2CH_2NH_2 \rightarrow CH_3S+CH_2CH_2CH_2NH_2 \rightarrow CH_3S+CH_2CH_2+CH_2NH_2$, the dissociation processes are different. One starts from S–C bond cleavage followed by C–C bond fission, the other starts from the reverse sequence. In fact, the dissociation starting from C–C bond cleavage can be excluded from the velocity distributions of fragments $m/e=30$ and 47. This is because the velocity distribution of $m/e=30$ is very broad, but the velocity distribution of $m/e=47$ has two components. If the dissociation starts from C–C bond cleavage, the velocity distribution of $m/e=75$ must be very broad because $m/e=30$ and 75 are from the same process. Then, it is impossible to generate the two-component velocity distribution of the secondary product $m/e=47$ from a broad velocity distribution of $m/e=75$.

The photofragment translational energy distributions obtained from the images are shown in Fig. 3. For H atom elimination channel, it shows that the average released translational energy is large, and the peak of the distribution is located at 25 kcal/mol. It is interesting to note that the maximum translational energy almost reaches the maximum available energy of the reaction $CH_3SCH_2CH_2CH_2NH_2 \rightarrow CH_3SCH_2CH_2CH_2NH+H$. For both CH_3 elimination and CH_3S elimination channels, the translational energy distribution shows two components. The average released translational energies of the fast components are large, and the peaks of the fast components are located at 40 and 20 kcal/mol, respectively. The maximum translational energy (~65 kcal/mol) of the fast component from CH_3 elimination almost reaches the maximum available energy (76 kcal/mol) of the corresponding reactions. However, the maximum translational energy (~40 kcal/mol) in the CH_3S elimination channel is about 40 kcal/mol less than the available energy. This indicates that a lot of energy is distributed in the internal degrees of freedom of the fragments. As a result, the fragments can easily undergo secondary dissociation. This provides the explanation that the corresponding fragment $m/e=58$ was not observed. On the other hand, there is only one component in the translational energy distribution of reaction $CH_3SCH_2CH_2CH_2NH_2 \rightarrow CH_3SCH_2+CH_2CH_2NH_2$. The peak of the distribution is very close to zero and the probability decreases with the increase of the translational energy.

B. Cysteamine

The fragment ion images are shown in Fig. 4. Both fragment $m/e=33$ and 44 have line shape images and they contain a fast and a slow component. The slow component of fragments $m/e=44$ has the same intensity profile as $m/e=43$, indicating $m/e=43$ from the dissociation or dissociative ionization of $m/e=44$. This is similar to the fragment cracking of $m/e=44$ observed in 3-(methylthio)propylamine as described in the previous section. The momentum distributions between $m/e=33$ and the sum of $m/e=43$ and 44 match very well, indicating the HS elimination channel. In addition, ions of $m/e=30$, 46, and 47 were observed. The image profiles of $m/e=46$ and 47 are very similar. The momentum distributions between $m/e=46$ and 30 match very well if $m/e=46$ is assumed from the dissociative ionization of $m/e=47$. It indicates the dissociation channel of C–C bond cleavage.

The photofragment translational energy distributions obtained from the images are shown in Fig. 5. For HS elimination channel, the translational energy distribution shows two

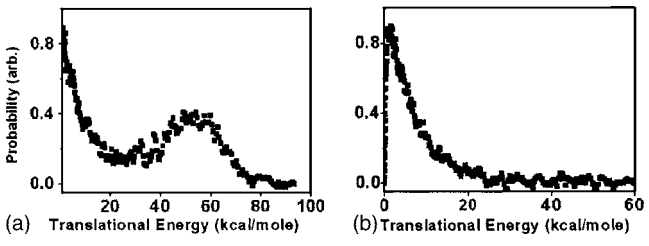

FIG. 5. Translational energy distribution of reaction (a) $HSCH_2CH_2NH_2 \rightarrow HS+CH_2CH_2NH_2$ and (b) $HSCH_2CH_2NH_2 \rightarrow HSCH_2+CH_2NH_2$.

TABLE II. Branching ratios from RRKM calculations. Only dissociations from the ground electronic state are taken into consideration.

Reaction	Branching ratio
$CH_3SCH_2CH_2CH_2NH_2 \rightarrow CH_3SCH_2CH_2CH_2NH+H$	0
$CH_3SCH_2CH_2CH_2NH_2 \rightarrow CH_3+SCH_2CH_2CH_2NH_2$	0.40
$CH_3SCH_2CH_2CH_2NH_2 \rightarrow CH_3S+CH_2CH_2CH_2NH_2$	0.48
$CH_3SCH_2CH_2CH_2NH_2 \rightarrow CH_3SCH_2+CH_2CH_2NH_2$	0.06
$CH_3SCH_2CH_2CH_2NH_2 \rightarrow CH_3SCH_2CH_2+CH_2NH_2$	0.02
$CH_3SCH_2CH_2CH_2NH_2 \rightarrow CH_3SCH_2CH_2CH_2+NH_2$	0.04
$HSCH_2CH_2NH_2 \rightarrow H+SCH_2CHNH_2$	0
$HSCH_2CH_2NH_2 \rightarrow HS+CH_2CH_2NH_2$	0.55
$HSCH_2CH_2NH_2 \rightarrow HSCH_2+CH_2NH_2$	0.16
$HSCH_2CH_2NH_2 \rightarrow HSCH_2CH_2+NH_2$	0.15
$HSCH_2CH_2NH_2 \rightarrow HSCHCH_2+NH_3$	0.06
$HSCH_2CH_2NH_2 \rightarrow HSCH_3+CHNH_2$	0.04

components. The average translational energy of the fast component is large, and the peak of the distribution is located at 50 kcal/mol. The maximum translational energy of the fast component also reaches the maximum available energy of the corresponding reactions. On the other hand, there is only a small amount of energy released into the translational energy in the C–C bond cleavage, and the peak of the distribution is very close to zero.

V. DISCUSSION

For 3-(methylthio)propylamine, the results can be described as the following reactions:

$$CH_3SCH_2CH_2CH_2NH_2 \rightarrow CH_3SCH_2CH_2CH_2NH + H, \quad (1)$$

$$CH_3SCH_2CH_2CH_2NH_2 \rightarrow CH_3 + SCH_2CH_2CH_2NH_2, \quad (2)$$

$$CH_3SCH_2CH_2CH_2NH_2 \rightarrow CH_3S + CH_2CH_2CH_2NH_2, \quad (3)$$

$$CH_3SCH_2CH_2CH_2NH_2 \rightarrow CH_3SCH_2 + CH_2CH_2NH_2. \quad (4)$$

Most of the fragments $CH_2CH_2CH_2NH_2$ decompose into smaller fragments $CH_2CH_2+CH_2NH_2$, and part of the fragments $CH_2CH_2NH_2$ decompose into CH_2CHNH_2+H. For cysteamine, the results can be described as the following reactions:

$$HSCH_2CH_2NH_2 \rightarrow HS + CH_2CH_2NH_2, \quad (5)$$

$$HSCH_2CH_2NH_2 \rightarrow HSCH_2 + CH_2NH_2. \quad (6)$$

Part of the fragments $CH_2CH_2NH_2$ and $HSCH_2$ decompose into smaller fragments CH_2CHNH_2+H and SCH_2+H, respectively. The relative branching ratios for various dissociation channels from the ground electronic state are predicted by RRKM calculations. They are listed in Table II. Most of the major channels predicted by calculations were observed in the experiment. The ion intensity ratios for various fragments are listed in Table III. The values have been corrected for the fragment velocity effect, and the relative branching ratios can be obtained directly from the normalization of these values by the ionization cross sections at this wavelength.

Unfortunately most of the relative ionization cross sections of these radicals are not available from literature at this moment. We obtained the relative ionization cross sections of CH_3 and SCH_3 at 118.2 nm from the following measurement. In the photodissociation of dimethyl sulfide CH_3SCH_3, one of the major channels is $CH_3SCH_3 \rightarrow CH_3S+CH_3$. The relative ion intensity between $CH_3S^+ + CHS^+$ (due to fragment cracking upon ionization) and CH_3^+ measured by the same VUV wavelength (118.2 nm) is 15.4:1. Since these two fragments results from the same dissociation channel of dimethyl sulfide and the VUV photon energy is much higher than the ionization potential of these two fragments, the relative ion intensity gives a good estimation of the relative ionization cross section of these two fragments at this VUV laser wavelength. This ratio can be used to calculate the relative branching ratio between reactions (2) and (3). For the other channels, the ion intensity ratios obtained from this experiment only provide a very crude estimation for comparison with the calculation. Note that the branching ratios

TABLE III. Fragment relative ion intensity at 118 nm and branching ratios.

3-(methylthio)propylamine								
	15		30	43	45+47		61	104
m/e	slow	fast	slow	slow	slow	fast	slow	fast
Ion intensity	0.01	0.07	0.25	0.31	0.4	0.6	0.13	0.007
Branching ratio	0.25	1.75			0.67	1.0		

Cysteamine			
	43+44		46+47
m/e	slow	fast	slow
Ion intensity	1.4	2	1

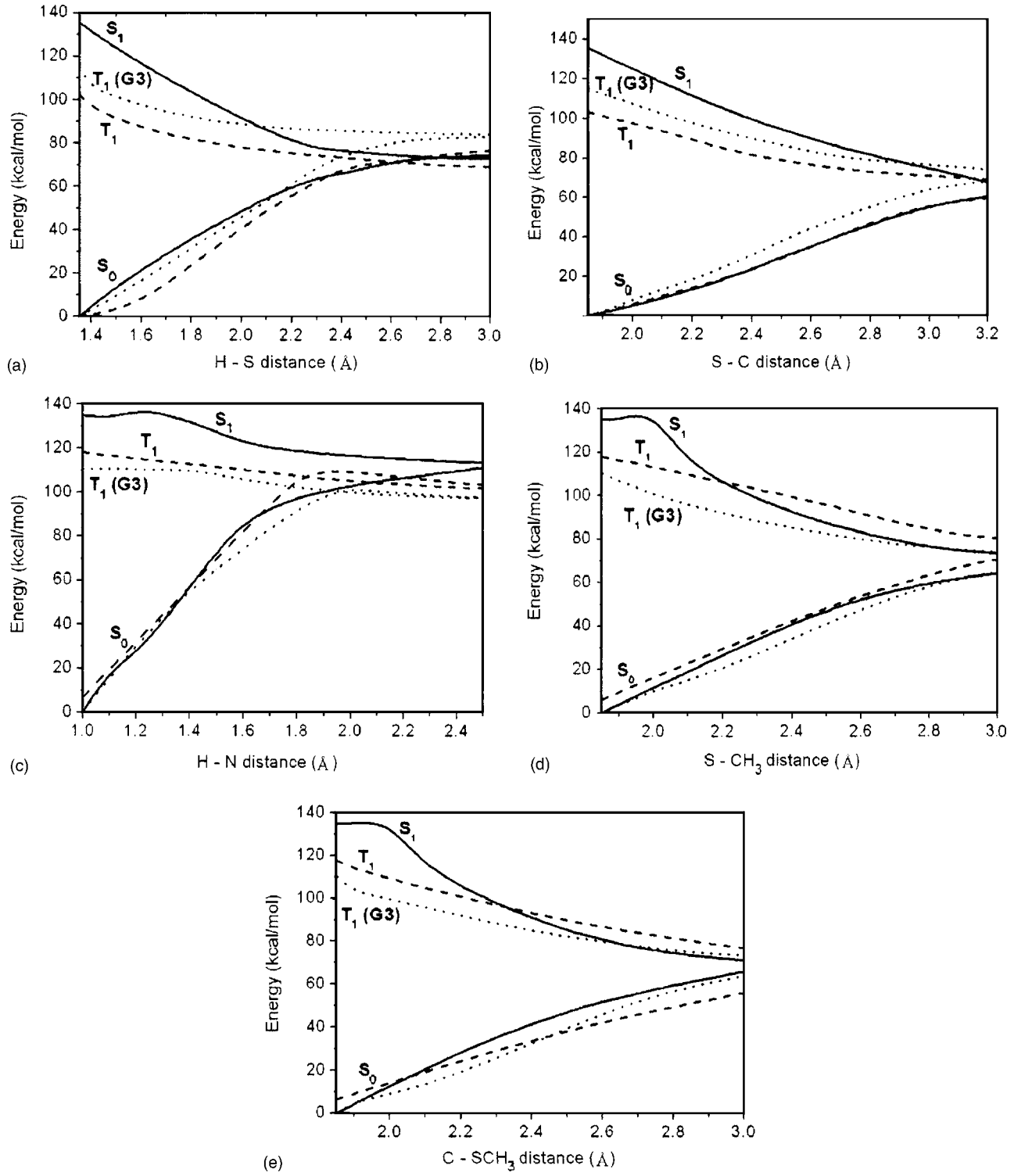

FIG. 6. Potential energy curves electronic ground state (S_0), the first singlet (S_1) and triplet (T_1) states along (a) H–S bond distance of C_2H_7NS (C–S distance is fixed), (b) C–S bond distance of C_2H_7NS (H–S distance is fixed), (c) N–H bond distance of $C_4H_{11}NS$ (C–SCH_3 and S–CH_3 distances are fixed), (d) S–CH_3 bond distance of $C_4H_{11}NS$ (C–SCH_3 distance is fixed), and (e) C–SCH_3 bond distance of $C_4H_{11}NS$ (S–CH_3 distance is fixed). Solid lines are the MRCI S_1 and S_0 energies, where S_0 energy was calculated at the S_1 optimized geometry. Dashed lines are the MRCI T_1 and S_0 energies, where S_0 energy was calculated at the T_1 optimized geometry. Dotted lines are the T_1 and S_0 energies, calculated by the G3 computational scheme. S_0 energy was calculated at the T_1 optimized geometry, founded by the B3LYP/6-31G* method.

from RRKM calculation only take the dissociation from the ground state into account. Therefore, only the slow component of the ion intensity can be compared to the calculation results. The experimental measurement of the relative branching ratio of reactions (2) and (3) is 0.25/0.67=0.37. The relative branching ratio from RRKM calculation is 0.4/0.48=0.83, which is close to the experimental measurement.

The translational energy distributions we observed from these dissociation channels can be classified into two types.

One has the peak of the distribution very close to zero. This is the typical characteristic of dissociation from a molecule undergo internal conversion to the ground electronic state with no exit barrier. This type of translational energy distribution was observed from reactions (4) and (6), and the slow components of reactions (2), (3), and (5). For the other type of distribution, the peak of the distribution is located far away from zero, and the maximum translational energy distribution almost reaches the maximum available energy of the reaction. These are characteristic of dissociation from a repulsive excited state, or dissociation from an electronic state with a large exit barrier. This type of translational energy distribution was observed from reaction (1) and the fast components of reactions (2), (3), and (5).

For the reaction $CH_3SCH_2CH_2CH_2NH_2 \rightarrow CH_3 + SCH_2CH_2CH_2NH_2$ in the electronic ground state, *ab initio* calculation (B3LYP/6-31+G*) shows that the methyl group changes gradually from pyramidal geometry to planar geometry as the C–C bond length increases during the dissociation process. There is no exit barrier for the dissociation from the ground state. No exit barrier was also found for the other channels in the electronic ground state. This indicates that the slow components in the translational energy distributions result from the ground state dissociation and the fast components do *not* result from the ground state dissociation. The fast components must result directly from a repulsive state, or from the coupling between the stable and repulsive states, or a lower electronic state with a large exit barrier.

Indeed, our *ab initio* calculations show the existence of the electronic excited state with a repulsive potential energy surface along the dissociating bond distance. Figure 6 illustrates that repulsive potential energy surfaces were found for every dissociation channels with large translational energy release. Both the singlet excited state and the triplet state were found to be repulsive. The singlet excited state can be achieved by photoexcitation, and the triplet state can be reached after intersystem crossing due to the spin-orbit effect of the S atom. These excited states are also located within the energy region that can be reached by 193 nm photoexcitation. This confirms our proposed dissociation mechanism that the fast component must result from the repulsive state.

The existence of the electronic excited states with repulsive potential energy surfaces along the S–R (R=H, CH_2, or CH_3) bond distance has been observed in the other small S containing molecules. For example, $CH_3SH \rightarrow CH_3+SH$ and $CH_3SH \rightarrow CH_3S+H$ are the major dissociation channels in the photodissociation of CH_3SH at 193 nm.[41,42] The peaks of the translation energy distributions are located at 50 and 40 kcal/mol for these two channels, respectively. The maximum translational energy releases also reach the maximum available energy of each channel. These indicate a repulsive potential energy surface that can be accessed by 193 nm photoexcitation directly or indirectly. Similar translational energy distributions were found from the S–C bond cleavage of the others containing molecules such as CH_3SCH_3 and $HSCH_2CH_2SH$ at 193 nm.[43–45]

Ammonial (Ref. 46) and its methyl-substituted derivatives[47,48] have been studied as examples of small molecules containing amino group. The UV photodissociation of these molecules demonstrated that N–R (R=H, CH_3) bond cleavage from amino group is the major channel. The first singlet excited state of these molecules is predissociated by an $n \rightarrow \sigma^*$ state, leading to the fission of N–R bond from the repulsive excited state. In addition to these small amines, the N–H bond dissociation from a repulsive excited state also has been observed from the photodissociation of aniline, $C_6H_5NH_2$, at 193 nm.[49]

In conclusion, we demonstrated that the dissociation from the repulsive excited state plays an important role in the S atom containing amino acid chormophores at this wavelength. The existence of the repulsive excited state must be related to the electronic structures of S atom and the C atoms in the neighborhood. The excited state has a significant antibonding σ^* character with respect to the S–C bond, and it can be reached by 193 nm photoexcitation. The location of this excited state does not change much from one molecule to the other molecule. On the other hand, the excited state of a significant antibonding σ^* character with respect to the N–H bond was only observed in 3-(methylthio)propylamine. No corresponding dissociation was observed in cysteamine. Although the observation was made in the gas phase under collisionless conditions, the dissociation from the excited state with a repulsive potential energy surface is very fast and it would not be quenched completely even in the condensed phase. These dissociation channels must play important roles in the condensed phase.

[1] M. B. Robin, *Higher Excited States of Polyatomic Molecules* (Academic, New York, 1972).
[2] C. E. Crespo-Hernandez, B. Cohen, P. M. Hare, and B. Kohler, Chem. Rev. (Washington, D.C.) **104**, 1977 (2004).
[3] R. Callis, Annu. Rev. Phys. Chem. **34**, 329 (1983).
[4] D. Creed, Photochem. Photobiol. **39**, 537 (1984).
[5] A. Reuther, H. Iglev, R. Laenen, and A. Laubereau, Chem. Phys. Lett. **325**, 360 (2000).
[6] A. L. Sobolewski, W. Domcke, C. Dedonder-Lardeuxc, and C. Jouvet, Phys. Chem. Chem. Phys. **4**, 1093 (2002).
[7] Z. Lan, W. Domcke, V. Vallet, A. L. Sobolewski, and S. Mahapatra, J. Chem. Phys. **122**, 224315 (2005).
[8] A. L. Sobolewski and W. Domcke, J. Phys. Chem. A **105**, 9275 (2001).
[9] R. J. Lipert, G. Bermudez, and S. D. Colson, J. Phys. Chem. **92**, 3801 (1988).
[10] J. A. Syage, Z. Phys. D: At., Mol. Clusters **30**, 1 (1994).
[11] N. Mikami, Bull. Chem. Soc. Jpn. **68**, 683 (1995).
[12] T. S. Zwier, Annu. Rev. Phys. Chem. **47**, 205 (1996).
[13] R. M. Helm, H. P. Vogel, and H. J. Neusser, J. Chem. Phys. **11**, 4496 (1998).
[14] G. Pino, G. Grégoire, D. Dedonder-Lardeux, C. Jouvet, S. Martrenchard, and D. Solgadi, Phys. Chem. Chem. Phys. **2**, 893 (2000).
[15] S. Ishiuchi, K. Daigoku, M. Sakai, K. Hashimoto, and M. Fujii, J. Chem. Phys. **117**, 7083 (2002).
[16] O. David, C. Dedonder-Lardeux, and C. Jouvet, Int. Rev. Phys. Chem. **21**, 499 (2002).
[17] Y. Yamada, T. Ebata, M. Kayano, and N. Mikami, J. Chem. Phys. **120**, 7400 (2004).
[18] M. Kayano, T. Ebata, Y. Yamada, and N. Mikami, J. Chem. Phys. **120**, 7410 (2004).
[19] C. M. Tseng, Y. T. Lee, and C. K. Ni, J. Chem. Phys. **121**, 2459 (2004); M. G. D. Nix, A. L. Devine, B. Cronin, R. N. Dixon, and M. N. R. Ashfold, *ibid.* **125**, 133318 (2006).
[20] M. F. Lin, C. M. Tseng, Y. T. Lee, and C. K. Ni, J. Chem. Phys. **123**, 124303 (2005); A. L. Devine, B. Cronin, M. G. D. Nix, and M. N. R. Ashfold, *ibid.* **125**, 184302 (2006).
[21] R. Hermann, G. R. Mahalaxmi, T. Jochum, S. Naumov, and O. Brede, J. Phys. Chem. A **106**, 2379 (2002).
[22] E. J. Land, P. Porter, and E. Strachan, Trans. Faraday Soc. **57**, 1885

(1961).
[23] E. J. Land and G. Porter, Trans. Faraday Soc. **59**, 2016 (1963).
[24] S. Dellonte, G. Marconi, and S. Monti, J. Photochem. **39**, 33 (1987).
[25] D. V. Bent and E. Hayon, J. Am. Chem. Soc. **97**, 2599 (1975).
[26] G. Grabner, G. Köhler, G. Marconi, S. Monti, and E. Venuti, J. Phys. Chem. **94**, 3609 (1990).
[27] O. Brede, H. Orthner, V. Zubarev, and R. Hermann, J. Phys. Chem. **100**, 7097 (1996).
[28] R. Hermann, S. Naumov, and O. Brede, J. Mol. Struct.: THEOCHEM **532**, 69 (2000).
[29] S. T. Tsai, C. K. Lin, Y. T. Lee, and C. K. Ni, J. Chem. Phys. **113**, 67 (2000).
[30] S. T. Tsai, C. L. Huang, Y. T. Lee, and C. K. Ni, J. Chem. Phys. **115**, 2449 (2001).
[31] S. T. Tsai, C. K. Lin, Y. T. Lee, and C. K. Ni, Rev. Sci. Instrum. **72**, 1963 (2001).
[32] C. K. Lin, C. L. Huang, J. C. Jiang, H. Chang, S. H. Lin, Y. T. Lee, and C. K. Ni, J. Am. Chem. Soc. **124**, 4068 (2002).
[33] C. L. Huang, J. C. Jiang, A. M. Mebel, Y. T. Lee, and C. K. Ni, J. Am. Chem. Soc. **125**, 9814 (2003).
[34] C. K. Ni and Y. T. Lee, Int. Rev. Phys. Chem. **23**, 187 (2004).
[35] (a) L. A. Curtiss, K. Raghavachari, P. C. Redfern, V. Rassolov, and J. A. Pople, J. Chem. Phys. **109**, 7764 (1998); (b) A. G. Baboul, L. A. Curtiss, P. C. Redfern, and K. Raghavachari, *ibid.* **110**, 7650 (1999); (c) L. A. Curtiss, K. Raghavachari, P. C. Redfern, A. G. Baboul, and J. A. Pople, Chem. Phys. Lett. **314**, 101 (1999).
[36] A. D. Becke, J. Chem. Phys. **96**, 2155 (1992); **97**, 9173 (1992); **98**, 5648 (1993).
[37] C. Lee, W. Yang, and R. G. Parr, Phys. Rev. B **37**, 785 (1988).
[38] W. J. Hehre, R. Ditchfield, and J. A. Pople, J. Chem. Phys. **56**, 2257 (1972).
[39] V. V. Kislov, T. L. Nguyen, A. M. Mebel, S. H. Lin, and S. C. Smith, J. Chem. Phys. **120**, 7008 (2004).
[40] N. R. Forde, L. Butler, B. Ruscic, O. Sorkhabi, F. Qi, and A. Suits, J. Chem. Phys. **113**, 3088 (2000).
[41] W. A. Chupka and C. Lifshitz, J. Chem. Phys. **48**, 1109 (1968).
[42] S. Nourbakhsh, K. Norwood, H. M. Yin, C. L. Liao, and C. Y. Ng, J. Chem. Phys. **95**, 946 (1991).
[43] E. Jensen, J. S. Keller, G. C. G. Waschewsky, J. E. Stevens, R. L. Graham, K. F. Freed, and L. J. Butler, J. Chem. Phys. **98**, 2882 (1993).
[44] Y. R. Lee, C. L. Chiu, and S. M. Lin, J. Chem. Phys. **100**, 7376 (1994).
[45] H. Q. Zhao, Y. S. Cheung, C. X. Liao, C. Y. Ng, W. K. Li, and S. W. Chiu, J. Chem. Phys. **104**, 130 (1996).
[46] J. Biesner, L. Schnieder, G. Ahlers, X. Xie, K. H. Welge, M. N. R. Ashfold, and R. N. Dixon, J. Chem. Phys. **91**, 2901 (1989).
[47] G. C. G. Waschewsky, D. C. Kitchen, P. W. Browning, and L. J. Butler, J. Phys. Chem. **99**, 2635 (1995).
[48] N. R. Forde, M. L. Morton, S. L. Curry, S. J. Wrenn, and L. J. Butler, J. Chem. Phys. **111**, 4558 (1999).
[49] C. M. Tseng, Y. A. Dyakov, C. L. Huang, A. M. Mebel, S. H. Lin, Y. T. Lee, and C. K. Ni, J. Am. Chem. Soc. **126**, 8760 (2004).